Direct Visualization of Heterogeneous Extravascular Distribution of Trastuzumab in Human Epidermal Growth Factor Receptor Type 2 Overexpressing Xenografts

Jennifer H.E. Baker, Kirstin E. Lindquist, Lynsey A. Huxham, Alastair H. Kyle, Jonathan T. Sy, and Andrew I. Minchinton

Abstract

Purpose: The high molecular weight and binding affinity of trastuzumab, a monoclonal antibody in use for treatment of breast cancers overexpressing human epidermal growth factor receptor type 2 (HER2), in combination with microenvironmental factors, may limit its distribution and efficacy. We assessed and mapped the distribution of systemically given, unlabeled trastuzumab at micrometer resolution in tumor xenografts using immunohistochemistry.

Experimental Design: Mice bearing MDA-435/LCC6^{HER2} xenografts were given single doses of 4 or 20 mg/kg unlabeled trastuzumab with tumor harvest at various time points thereafter; bound trastuzumab was imaged directly in tumor cryosections using fluorescently tagged anti-human secondary antibodies. Combinations of additional markers, including HER2, 5-bromo-2-deoxyuridine, CD31, DioC_7(3), desmin, and collagen IV were also mapped on the same tumor sections.

Results: Distribution of trastuzumab in MDA-435/LCC6^{HER2} tumors is found to be heterogeneous, with tumor margins saturating more thoroughly in doses and times analyzed. Considerable intervessel heterogeneity is also seen. For example, in unsaturated tissues, there remain perfused vessels without any trastuzumab in addition to vessels with a few layers of positively stained perivascular cells, in addition to vessels with bound drug up to 150 μm away. This heterogeneity is independent of HER2 expression, microvessel density, and perfusion. A slightly greater proportion of vessels were associated with pericytes in sections with greater trastuzumab saturation, but this would not adequately account for observed heterogeneous trastuzumab distribution.

Conclusions: Complete penetration of trastuzumab in tumor tissue was not seen in our study, leaving the possibility that inadequate distribution may represent a mechanism for resistance to trastuzumab.

Many anticancer agents may have limited efficacy due to their inability to distribute in tumor tissue and expose all cells to therapeutic doses (1). Tumor cells exhibit uneven responses to anticancer therapy due to their proximity to vasculature and microenvironment where factors such as oxygen and nutrient availability influence drug sensitivity. Tumor vascular abnormalities that contribute to inefficient drug penetration include large and variable intervascular distances, complex and tortuous branching patterns, lack of lymphatic vessel drainage, and irregular vascular phenotypes related to maturity, angiogenic capacity, size, perfusion, and permeability (for a review, see ref. 2). These contributing abnormalities create regions of irregular or intermittent blood flow, slowed interstitial fluid velocity, and often elevated interstitial fluid pressure (3). The extravascular compartment of tumors is also highly variable and abnormal, with tumor-specific extracellular matrix density, characteristics and expression patterns (4–6), presence or absence of stromal tissues, such as inflammatory cells (7), and altered tumor cell expression of antigen, receptors (8), or structures for transport of drug into or out of tumor cells (9).

With this veritable gauntlet of factors capable of inhibiting access of drugs to their target tumor cells, in addition to pharmacokinetic variable such as consumption and metabolism of diffusing drugs, it is not surprising that many small molecule cancer therapeutics have shown evidence of poor tumor tissue penetration in both *in vitro* and *in vivo* model systems, including doxorubicin (10), gemcitabine (11), docetaxel, and paclitaxel (ref. 12; for a recent review, see ref. 1). Monoclonal antibodies can face added difficulties due to their high molecular weights, target specificity, kinetics of metabolism and internalization, as well as the patterns of antigen expression in combination with target-binding affinity (13, 14).

Authors' Affiliation: Medical Biophysics Department, British Columbia Cancer Research Center, Vancouver, British Columbia, Canada

Received 9/27/07; revised 12/17/07; accepted 12/19/07.

Grant support: Canadian Breast Cancer Foundation and Canadian Institutes of Health Research. J.H.E. Baker and L.A. Huxham are Michael Smith Foundation for Health Research scholars. A.H. Kyle is a Michael Smith Foundation for Health Research and Canadian Institutes of Health Research scholar.

The costs of publication of this article were defrayed in part by the payment of page charges. This article must therefore be hereby marked *advertisement* in accordance with 18 U.S.C. Section 1734 solely to indicate this fact.

Note: Jennifer H.E. Baker and Kirstin E. Lindquist contributed equally to this article.

Requests for reprints: Andrew I. Minchinton, Department of Medical Biophysics, British Columbia Cancer Research Center, 675 West 10th Avenue, Vancouver, British Columbia, V5Z 1L3, Canada. Phone: 604-675-8032; Fax: 604-675-8049; E-mail: aim@bccrc.ca.

doi:10.1158/1078-0432.CCR-07-4465

The human epidermal growth factor receptor type 2 (HER2) is overexpressed in 20% to 30% of all invasive breast carcinomas and is a prognostic factor of an aggressive tumor phenotype, increased relapse, and decreased overall survival (15). HER2 status is determined in patient tissue samples by pathologic analysis using fluorescence *in situ* hybridization and immunohistochemistry; patients classified as positive for HER2-overexpressing breast cancer are candidates for, and have been shown to benefit from, therapy that includes a humanized monoclonal antibody against HER2, trastuzumab (Roche; refs. 16–19).

Several methods for investigating extravasation and tissue penetration of HER2-targeting antibodies and antibody fragments have been previously reported, including the use of fluorescent or radiolabeled drug preparations for imaging of tumor sections (20), intravital scintigraphic imaging (21), single-photon emission computed tomography (22), positron emission tomography (23), and magnetic resonance imaging (24). Additionally, the *in vivo* pharmacokinetics of trastuzumab have been analyzed at the single-molecule level using trastuzumab-conjugated fluorescent nanoparticles, called Q-dots, along with intravital imaging (25). Such studies can provide practical insight regarding strategies for the design of new immunotherapeutics and for the optimization of dosing and delivery regimes to result in maximal tissue penetration.

In this study, we show a quantitative approach to the study of trastuzumab penetration in tumors by directly imaging systemically administered, unlabeled trastuzumab in xenograft tumors using fluorescently tagged anti-human secondary antibodies on tissue cryosections. The microregional location of bound trastuzumab is then mapped in relation to several microenvironmental features, including vasculature, indicators of microvessel structural and functional integrity, HER2 expression, and cellular proliferation. This is the first study describing distribution of unlabeled trastuzumab in the context of the tumor microenvironment at micrometer resolution.

Materials and Methods

Reagents. Trastuzumab (2.2 mg/mL; Hoffman-La Roche) was provided by the British Columbia Cancer Agency pharmacy; dilutions were prepared in sterile 0.9% NaCl before injection. 5-Bromo-2-deoxyuridine (BrdUrd; Sigma Chemical), 30 mg/mL solution in 0.9% NaCl, was used to label S-phase cells. The fluorescent dye $DioC_7(3)$ (Molecular Probes), 0.6 mg/mL dissolved in 75% (v/v) DMSO:25% sterile H_2O, was given i.v. as a marker of vessel perfusion (26).

Cells and cell culture. MDA-435/LCC6 cells (LCC6) and LCC6 cells stably transfected by electroporation with the mammalian expression vector pREP9 (Invitrogen) containing the 4.3-kb full-length human normal c-erbB2 cDNA to yield $LCC6^{HER2}$ or with the empty vector pREP9 to yield $LCC6^{Vector}$ cells were kindly provided by Dr. Wieslawa Dragowska (British Columbia Cancer Research Center). Cells were maintained as monolayers using MEM/EBSS (HyClone) supplemented with 10% bovine growth serum (HyClone) and passaged every 3 to 4 days. Cells were selected using media containing 500 μg/mL G418. Cellular HER2 overexpression was ascertained by flow cytometry, as previously described (27).

Mice and tumors. Female, nonobese, diabetic, severe combined immunodeficient NOD-SCID mice were bred and maintained in our institutional specific pathogen–free animal facility in accordance with the Canadian Council on Animal Care guidelines. The experiments described in this manuscript were approved by the Animal Care Committee of the University of British Columbia. Mice were allowed free access to standard laboratory rodent food and water and were used between 8 and 24 weeks of age, weighing between 20 and 28 g. $LCC6^{HER2}$ and $LCC6^{Vector}$ single cell suspensions (50 μL of 1.6×10^8 cells/mL) were implanted s.c. into the sacral region of mice. Mice were randomly assigned to experimental groups when their tumors reached 100 to 150 mm^3 as measured using calipers of three orthogonal diameters (a, b, and c) using the formula volume: $\pi/6(abc)$. Trastuzumab was administered via i.p. injection. Two hours before tumor excision, all mice were administered an S-phase marker at 1,500 mg/kg BrdUrd i.p.; 5 min before euthanasia and tissue excision, all mice were administered an i.v. perfusion marker of 75 μL 0.6 mg/mL $DioC_7(3)$.

Immunohistochemistry. Immediately after excision, tumors were frozen on an aluminum block held at -20°C, embedded in optimum cutting temperature (Tissue-TEK), and stored at -20°C until sectioning. All transverse sections were taken perpendicular to the cranial-caudal axis; serial step cryosections were obtained at 1-mm intervals. The general immunohistochemical procedure used has been previously reported (11). Briefly, 10-μm tumor cryosections were cut with a Cryostar HM560 (Microm International GmbH), air-dried, imaged for native $DioC_7(3)$ fluorescence, and fixed in 50% (v/v) acetone/methanol for 10 min at room temperature. All vasculature including nonperfused vessels, were identified using an antibody to PECAM/CD31 (BD PharMingen) with fluorescent Alexa 647 antirat secondary anti-body (Invitrogen). Trastuzumab was visualized using Alexa 546 antihuman secondary antibody (Invitrogen). Tissue sections were always imaged for trastuzumab before staining for HER2. HER2 not previously bound by trastuzumab was detected with a 1:10,000 dilution of 2.2 mg/mL trastuzumab and the same goat antihuman Alexa 546 secondary (Invitrogen) used for systemically given, bound trastuzumab detection. Pericytes were detected using a monoclonal antibody to desmin (clone D33, Signet antibodies) and fluorescent Alexa 488 antimouse secondary antibody (Invitrogen). Collagen IV was stained with a polyclonal antibody to collagen IV (Gene Tex) and antirabbit peroxidase-conjugated antibody (Sigma) developed with metal-enhanced 3,3′-diaminobenzidine substrate (Pierce). Slides stained for incorporated BrdUrd were treated with 4 mol/L HCl and neutralized in 0.1 mol/L sodium borate. Immunohistochemical detection used a monoclonal mouse anti-BrdUrd (clone BU33; Sigma) followed by an antimouse peroxidase-conjugated antibody (Sigma) and a metal-enhanced 3,3′-diaminobenzidine substrate (Pierce). Slides were then counterstained with hematoxylin, dehydrated, and mounted using Permount (Fisher Scientific) before imaging.

Image acquisition and overlay. The imaging system consisted of two set-ups (a and b): a robotic fluorescence microscope (axio Imager $Z1_a$ or IIIRS; $Zeiss_b$), monochrome CCD camera (Retiga 4000R, $Qimaging_a$; or model 4922, $Cohu_b$), and a motorized slide loader with x-y stage (Ludl Electronic $Products_a$), or a custom-built motorized x-y $stage_b$. Customized $ImageJ_a$ or NIH-Image $software_b$ (public domain program developed at the NIH[1]) running on $G5_a$ or $G3_b$ Macintosh computers (Apple Computers) allowed for automated tiling of adjacent microscope fields. Images of entire tumor cryosections up to 1 cm^2 were captured at a resolution of 0.75 μm_a or 1.0 μm_b per pixel. Grayscale images of trastuzumab and HER2 were overlaid using Adobe Photoshop CS (version 8.0); images of trastuzumab (green channel) and HER2 (red channel) were then combined using the darken mask, resulting in overlapped areas displayed as black. Grayscale CD31 and $DioC_7(3)$ images were thresholded, and a composite color image was produced (CD31 in dark blue prioritized over $DioC_7(3)$ in cyan) and overlaid on the images of trastuzumab (red) or combination images of HER2 (red) and trastuzumab (black).

Image analysis. Using the NIH-Image software application and user-supplied algorithms, fluorescent images were inverted and combinations of images of $DioC_7(3)$, CD31, D33, Coll IV, trastuzumab, HER2,

[1] http://rsb.info.nih.gov/ij

BrdUrd, and hematoxylin staining from each tumor section aligned and cropped to tumor tissue boundaries and staining artifacts were removed. Percentage of positive staining was obtained using the proportion of pixels at intensities meeting or exceeding a threshold value determined to be above background. For distribution analysis relative to vasculature, each pixel in an image was sorted based on its distance relative to CD31-positive vasculature, and the average tissue intensity, in 1.5-μm increments from vasculature, was determined for each tumor. Data is displayed as a combined average of a minimum of four tumors. Data was normalized by subtracting average intensities of control images at each distance. For dual positive-staining analysis of CD31 in combination with additional markers, thresholds were set to identify staining above background, and a minimum of 20% overlap was required to classify CD31 objects as dual labeled. Necrotic tissue was cropped out from hematoxylin-stained sections for all analysis listed above; the proportion of necrotic tissue was obtained by dividing the total number of pixels in images after cropping by the total number of pixels in whole-tumor areas. Where appropriate, charts display means ± SE.

Results

The distribution of trastuzumab within HER2 overexpressing xenografts was observed by examining tumors excised at a range of times after i.p. administration. Tumor cryosections were imaged and stained immunohistochemically for combinations of trastuzumab, HER2, endothelial cells, pericytes, collagen type IV, perfusion marker $DioC_7(3)$, and S-phase cells labeled with BrdUrd. Images of up to five markers were obtained from each tissue section.

Trastuzumab imaged directly in HER2 overexpressing xenografts in combination with immunohistochemical staining for HER2. Cryosections of MDA-435/LCC6^{HER2} xenografts from mice administered 20 mg/kg trastuzumab 3 h before tumor recovery (Fig. 1A and B) are compared with untreated tumors (Fig. 1C and D). Sections were imaged for the i.v. fluorescent dye, $DioC_7(3)$, (cyan) before immunostaining for CD31 (dark blue) and trastuzumab (black), which can be seen bound in the treated tumor at limited distances surrounding vasculature; note considerable intervessel heterogeneity with respect to the amount of associated trastuzumab (Fig. 1A). The same sections were subsequently stained for HER2, which is found to be present homogeneously throughout the field (Fig. 1B and D). Immunohistochemical staining for HER2 was done on tumors from all experiments to confirm relatively uniform expression (data not shown).

Distribution of trastuzumab over time. Mice bearing MDA-435/LCC6^{HER2} xenografts were given single i.p. doses of 4 mg/kg trastuzumab. Representative high resolution composite images for whole tumor sections obtained 2 to 2.5 mm from the tumor edge were generated as described above, with a magnified portion of an untreated control tumor shown in Fig. 2A. Similar images of treated tumors show trastuzumab staining (red) proximal to vasculature (CD31 in dark blue,

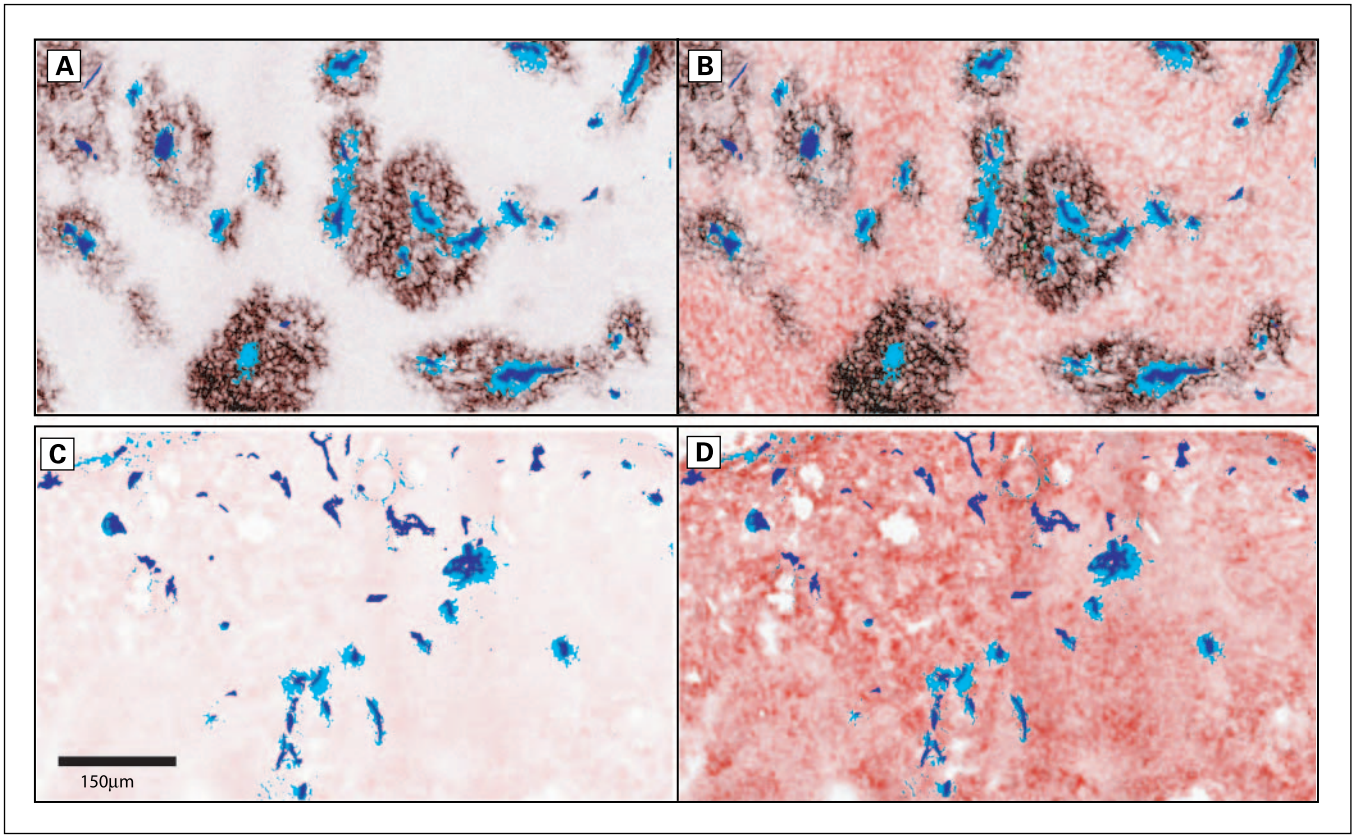

Fig. 1. Staining for bound trastuzumab and HER2. Tumor cryosections are shown from MDA-435-LCC6^{HER2}-overexpressing xenografts treated with 20 mg/kg trastuzumab for 3 h or left untreated. Overlaid images of a treated tumor show bound trastuzumab (*black*) relative to blood vessels (CD31; *dark blue*) and the perfusion marker $DioC_7(3)$ (*cyan*; *A*); additional staining of the same section for HER2 (*red*) shows that areas with no bound trastuzumab are overexpressing HER2 (*B*). An untreated MDA-435-LCC6^{HER2} tumor shows no bound trastuzumab (*C*) but relatively homogeneous HER2 expression (*D*). Similarly stained MDA-435-LCC6^{vector} tumors display no bound trastuzumab or unbound HER2 in treated or untreated tumors (not shown).

perfusion marker $DioC_7(3)$ in cyan) at 8 h (Fig. 2B), well distributed by 24 h (Fig. 2C), decreased in overall levels at 72 h (Fig. 2D), and barely detectable above control levels by 120 h (Fig. 2E). Quantitative analysis was done on whole tumor sections via selection of a threshold for bound trastuzumab staining; the extracellular binding pattern of this marker does not saturate all pixels representative of a cell, and therefore, the 15% positive tissue is not a reflection of the proportion of cells positive for bound trastuzumab but is instead a relative indication of amount of bound drug. Results indicate that after a 4 mg/kg dose, detectable levels are found as early as 3 h, with high levels of bound trastuzumab at 8 to 24 h compared with 72 to 120 h, wherein levels are reduced but are still above background (n = 5 per group; Fig. 2F).

Heterogeneous distribution of trastuzumab through whole tumors. Mice bearing MDA-435/LCC6^{HER2} xenografts were given a single dose of 20 mg/kg trastuzumab with tumor excision at 3 or 26 h. Transverse serial step cryosections (1-mm interval) were obtained for each tumor and were stained as described above. A greater proportion of tumor tissue positive for bound trastuzumab was found in marginal sections (1 mm from the tumor edge) compared with those from more central tumor sections (4 mm from the tumor edge) in both the 3 and 26 h time points, as shown in images of whole-tumor sections (Fig. 3A and B). Quantitative analysis of the percentage of pixels stained positively for trastuzumab above threshold is expressed as a function of distance from the tumor edge (Fig. 3C, *left*). Additional analysis determined the average intensity of trastuzumab staining as a function of distance from nearest microvessel; data shown are averages for a minimum of four tumors and are normalized by subtracting average untreated control intensities at each distance. After treatment, the average intensity throughout the tumor cord, up to 150 μm from vasculature, is lower in the sections 4 mm from the tumor edge compared with those only 1 mm from the edge in both the 3 and 26 h groups (Fig. 3C, *center* and *right*).

Qualitative observations of individual sections and close examination of bound trastuzumab around individual vessels

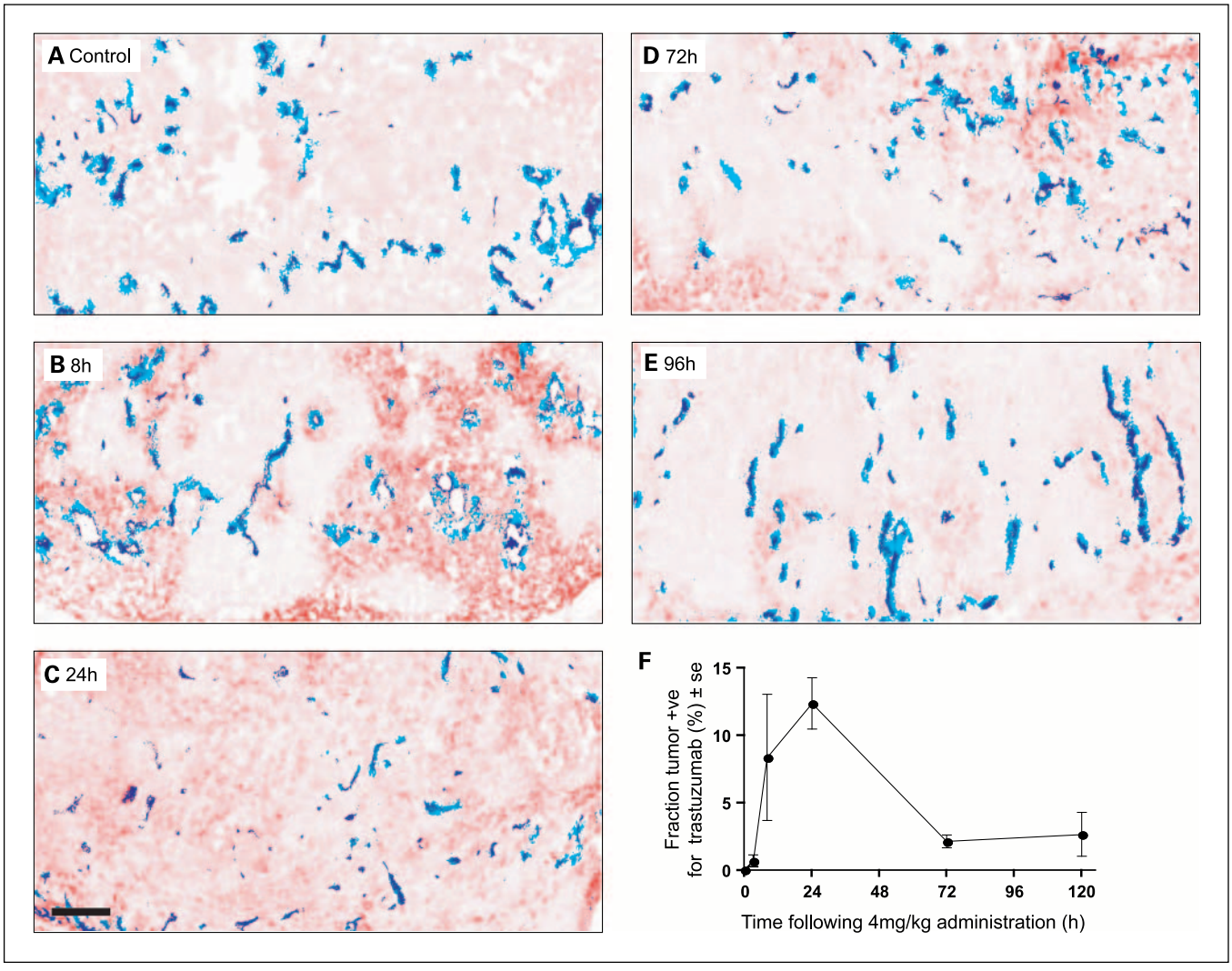

Fig. 2. Distribution of trastuzumab over time. The relative amount of bound trastuzumab in cryosections obtained 2 to 2.5 mm from the tumor edge of MDA-435-LCC6^{HER2} tumors is assessed using quantitative analysis of immunohistochemical staining. Representative portions of whole-tumor sections are shown with trastuzumab (*red*), CD31 (*dark blue*), and perfusion dye, $DioC_7(3)$ (*cyan*): an untreated control tumor (*A*), a single dose of 4 mg/kg trastuzumab at 8 h (*B*), 24 h (*C*), 72 h (*D*), and 96 h (*E*). The average fraction of tissue stained positively for bound trastuzumab shows detectable levels as early as 3 h, peak levels at 24 h, with significant decreases at 72 and 120 h (*F*).

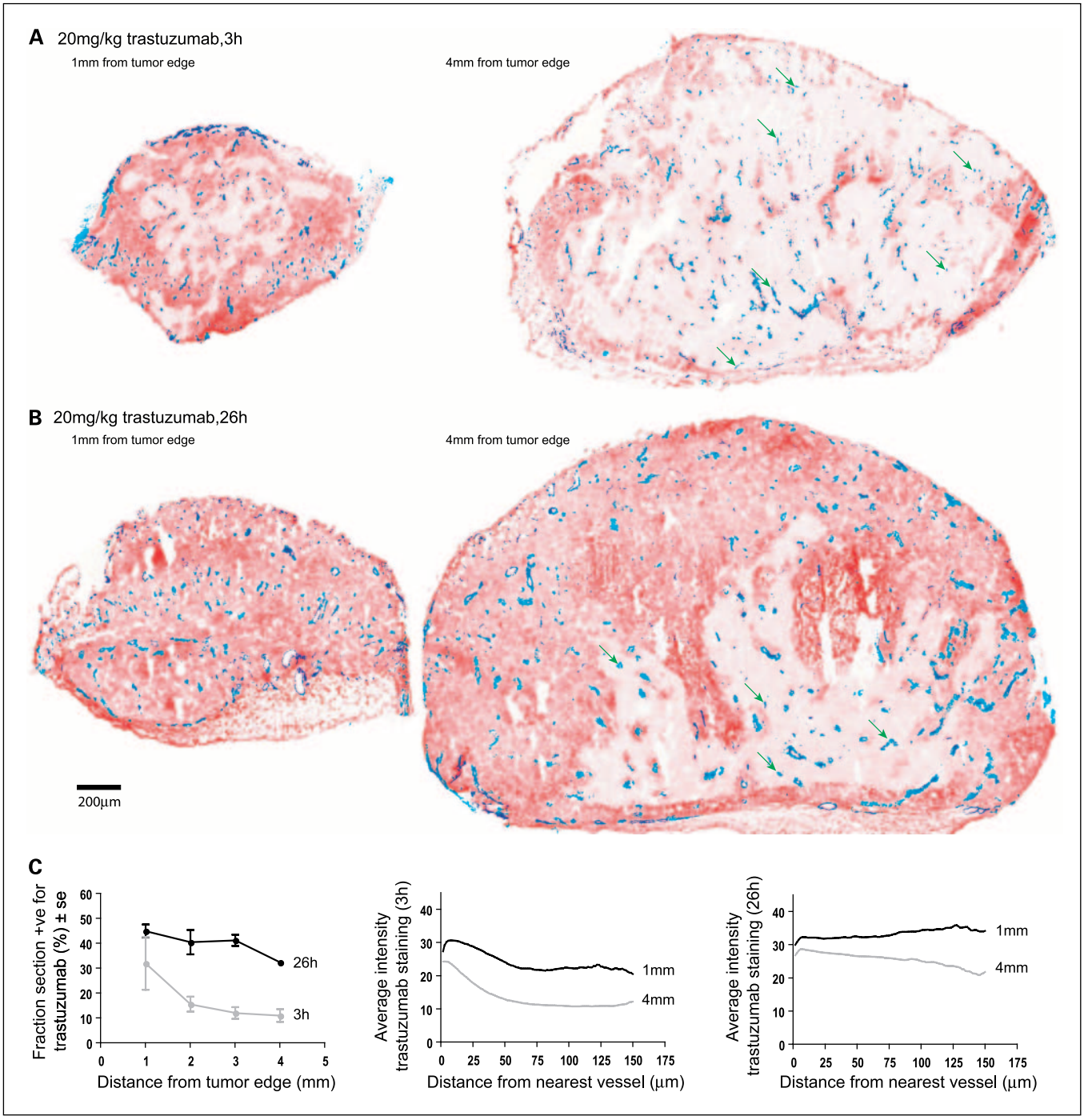

Fig. 3. Heterogeneous distribution of trastuzumab through whole tumors. Tumors grown to 8 to 10 mm in diameter were dosed with 20 mg/kg trastuzumab and harvested at 3 h (*A*) or 26 h (*B*); 10 μm thick transverse sections were obtained at 1 mm intervals from the tumor edge, were imaged for perfusion marker $DioC_7(3)$ (*cyan*), and stained for bound trastuzumab (*red*) and CD31 (*dark blue*). Examples of vessels with very little or no extravasating trastuzumab are illustrated (*green arrows*). Those sections obtained closer to the gross tumor edge of both the 3 h (*A, left*) and 26 h (*B, left*) show a greater proportion of tissue stained for trastuzumab than the more heterogeneous central sections (*A* and *B, right*). Quantitative analysis shows percentage of pixels positive for trastuzumab in sections at increasing distances from the tumor edge (*C, left*). The microregional distribution of trastuzumab as a function of distance from vasculature was analyzed on sections obtained 1 mm from tumor edge and compared with those at 4 mm; data is shown for tumors harvested at 3 h (*C, middle*) and 26 h (*C, right*) after treatment.

reveals considerable intervessel heterogeneity. For example, in tumors recovered just 3 h after trastuzumab administration, neighboring vessels that were perfused at the time of tumor recovery [CD31 objects also positive for $DioC_7(3)$] or seem to be similar in size may show varying amounts of bound trastuzumab ranging from just a few cell layers to up to 50 μm (Fig. 4A) or may in fact show no bound drug at all (arrows). In tissues that have unsaturated trastuzumab binding even at later time points, there can remain vessels without any trastuzumab (Fig. 3B, *arrows*), in addition to vessels with a few layers of perivascular cells staining positive for bound drug (Figs. 3B and 5B). Areas remaining unsaturated with trastuzumab were not consistently located in

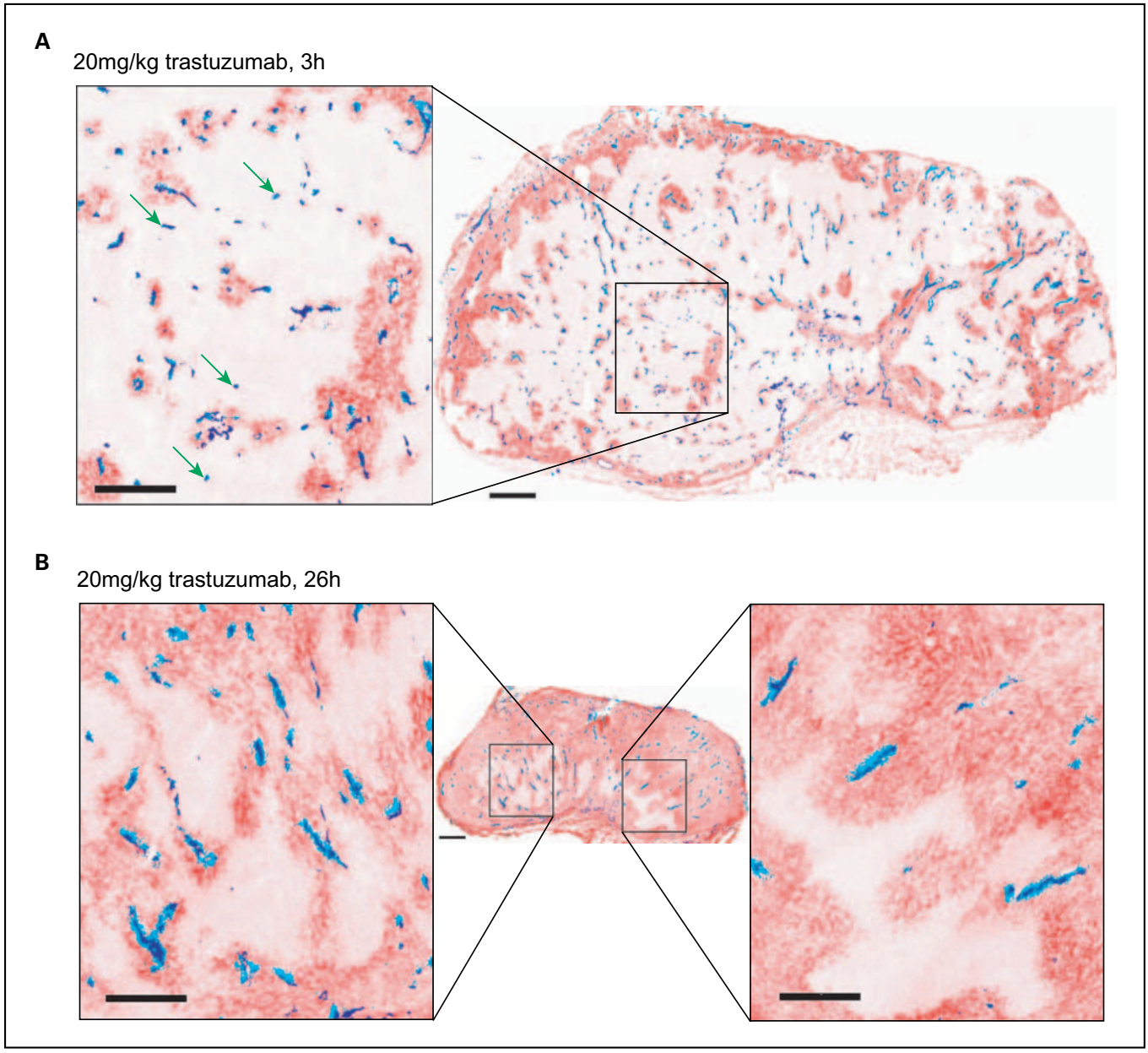

Fig. 4. Heterogeneous microregional distribution of trastuzumab. Tumors grown to 8 to 10 mm in diameter were dosed with 20 mg/kg trastuzumab and harvested at 3 h (*A*) or 26 h (*B*); 10 μm cryosections were imaged for perfusion marker $DioC_7(3)$ (*cyan*) and stained for bound trastuzumab (*red*) and CD31 (*dark blue*). Trastuzumab is seen to extravasate in a heterogeneous pattern in all regions of the tumor sections at 3 h (*A, right*); inset (*A, left*) illustrates presence of many perfused vessels not associated with significant amounts of trastuzumab (*green arrows*). At 26 h, tissue free of bound trastuzumab can still be found on cryosections (*B, middle*) in areas demonstrating both a high density of perfused vessels (*B, left*) and low density (*B, right*). All scale bars, 200 μm.

the center of tumor sections nor do they necessarily have low vascular density or lower rates of perfusion (Fig. 4B).

Vascular architectural features remain consistent throughout tumors with the exception of vascular association with pericytes. Tumor sections collected as above from mice treated with 20 mg/kg trastuzumab were stained for markers of vascular phenotype in serial step sections (1-mm interval) up to 4 mm from the tumor edge. No differences were found in microvascular density (Fig. 5A, *i*). Similarly, no difference was detected in the fraction of perfused vessels or vessels associated with presence of basal lamina, as detected by colocalization of CD31 and $DioC_7(3)$ or collagen IV, respectively (*ii* and *iii*). In contrast, a trend of increased association of D33 staining, a marker of pericytes, was found in association with CD31 in sections closest to the tumor edge (*iv*).

Tumor microenvironmental features do not significantly change after a single 4 mg/kg dose of trastuzumab. No significant microenvironmental changes were observed in MDA-435/$LCC6^{HER2}$ tumors at time points up to 120 h after a single 4 mg/kg dose of trastuzumab. Quantitative image analysis of cryosections obtained 2 to 2.5 mm from the tumor edge showed no change with time in microvessel density, the fraction of perfused vessels (Fig. 5B, *i*) or the fraction of BrdUrd incorporating cells analyzed as both percentage of

positive pixels (*ii*) or average intensity of staining as a function of distance from blood vessels (data not shown). Although the relative fraction of tissue identified as being necrotic by examination of hematoxylin-stained tissue did not change (*iii*), the fraction of necrotic tissue staining above threshold for bound trastuzumab does increase with time after treatment (*iv*).

Discussion

This study presents the first direct visualization of systemically administered trastuzumab in xenograft tumor tissue using immunohistochemistry, an approach that could be useful to many studies investigating distribution of monoclonal antibody therapeutics. This simple technique enabled qualitative and quantitative analysis of trastuzumab distribution to be assessed at high resolution in the context of additional tumor microenvironmental features, including HER2 expression, vasculature, and markers of vascular phenotype.

The tumor model MDA-435/LCC6^{HER2} is derived from the MDA-MB-435 cell line, which was formerly thought to be a human breast carcinoma, but genetic profiling has recently revealed it to have melanoma origins (28). The intention of the present study was to look at trastuzumab penetration and distribution in an *in vivo* preclinical model of tumor tissue overexpressing the HER2 antigen.

Trastuzumab has previously been shown to have anticancer efficacy against this tumor line (27), although results presented here show no changes in microvessel density, perfusion, proportion of S-phase tumor cells, or necrotic tissue were found up to 120 h after a single 4 mg/kg dose (Fig. 5A). It was noted, however, that the necrotic regions of treated tumors (72-120 h) had significant levels of bound trastuzumab, but it is unclear if this is a relevant phenomenon or an experimental artifact. Despite limited penetration of trastuzumab at some blood vessels, the majority of tissue is exposed to trastuzumab by 24 h, suggesting that if a measurable effect on tumor cell proliferation were to occur in this model under these conditions, it would be detectable in gross tissue analyses. However, this panel of markers assessing the effects of trastuzumab is not comprehensive and would not necessarily be expected to reflect its activity at such short time points after a single dose. The multimarker, serially immunostained model enabled simplified analysis of multiple markers per tumor section; future studies examining the effects of trastuzumab over prolonged periods with multiple dosage regimens may be able to use a similar system with these or additional pharmacodynamic markers to investigate mechanisms of activity of trastuzumab and relate them to the distribution and retention of bound drug or HER2 expression. Specific immunohistochemical techniques developed by Glazyrin et. al. (19) use trastuzumab as a primary antibody for the detection of HER2 status in untreated clinical samples despite the presence of additional human antibodies; it is possible that these same techniques could be extended to examine the distribution of bound trastuzumab, which could provide highly valuable data regarding the ability of trastuzumab to distribute and accumulate in treated patients.

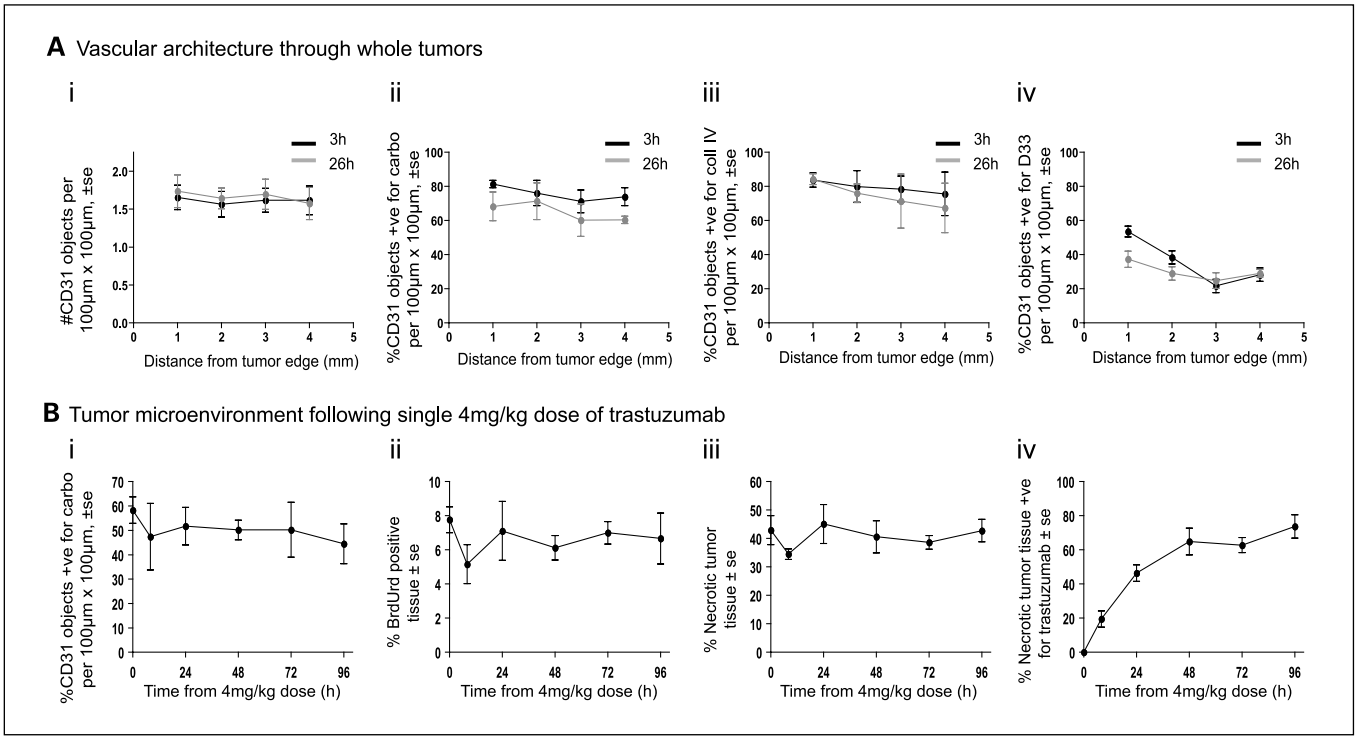

Fig. 5. Quantitative analysis of tumor microenvironment. Analyses of vascular architectural features were done on MDA-435-LCC6^{HER2} tumors treated with 20 mg/kg trastuzumab for either 3 or 26 h (*A*); transverse sections were obtained at 1 mm intervals from the tumor edge. No differences are seen in the density of CD31-stained microvessels (*Ai*), or the fraction of vessels staining dual positive for perfusion marker DioC$_7$(3) (*Aii*), or collagen type IV (*Aiii*); however, dual staining of CD31 with pericyte marker desmin D33 shows a decreasing trend at distances farther from the tumor edge (*Aiv*). Tumor microenvironmental features were also assessed at longer time points after a single 4 mg/kg dose of trastuzumab (*B*), with no significant changes in the fraction of perfused vessels (*Bi*), S-phase cells detected using BrdUrd incorporation (*Bii*), or the relative fraction of necrotic tumor tissue at time points up to 96 h after administration (*Biii*); however, the fraction of necrotic tissue that stains positive for bound trastuzumab does increase with time after treatment (*Biv*).

Accumulation of trastuzumab in tumor xenografts has previously been shown to reach peak concentrations within a few days of administration (20, 23, 29, 30) and substantial accumulation in the interstitial space has been detected at 2 h after administration (25). In this model, results are comparable with detectable levels as early as 3 h, significant levels at 8 to 24 h, and reduction by 72 h after a 4 mg/kg administration (Fig. 2). This dose was selected due to its use in previous studies with HER2-overexpressing xenograft tumors, as well as its similarity to clinically relevant doses (31, 32). These results suggest that the model used, MDA-435/LCC6^{HER2}, exhibits trastuzumab binding and metabolism characteristics similar to those seen in other models.

Microregional distribution of trastuzumab was found to be heterogeneous, with higher levels of bound drug found in transverse tissue sections obtained proximal to the tumor edge (1 mm) compared with more central sections (4 mm; Fig. 3). This heterogeneity is not explained by variable expression of HER2, which was found to be expressed in tumor tissues not bound by systemically administered trastuzumab (Fig. 1). Considerable intervessel heterogeneity was noted, wherein varying rates of extravasation and extravascular distribution of trastuzumab from tumor vessels were often seen (Figs. 4 and 5) in all areas of the tumor, often with neighboring vessels exhibiting completely different characteristics. Quantitative data was obtained to investigate whether vascular phenotype may be partially responsible for the greater degree of trastuzumab tissue saturation found in sections proximal to the tumor edge. A straightforward explanation for decreased trastuzumab binding in an area would be to show correspondingly lower vascular density or a lack of perfusion in existing vessels; however, analysis of microvessel density and the fraction of perfused vessels displayed no correlating trends through tumor tissue (Fig. 5A, *i* and *ii*). Intermittent changes to perfusion could affect the localized distribution of trastuzumab for individual vessels, although these temporal changes in blood flow are generally considered to be relatively infrequent and of short duration (33), and given the long half-life of trastuzumab, it is unlikely that intermittent perfusion changes could account for all of the heterogeneity seen with respect to trastuzumab distribution.

Many studies have illustrated the importance of extracellular matrix density and composition in the ability of macromolecules to distribute in the extravascular compartment of tumor tissue (4, 5, 34), although trastuzumab has been shown to have a relatively large interstitial volume of distribution in some tumor models (6). In this study, we examined the vascular extracellular matrix layer, the basal lamina, where the presence of collagen type IV showed consistent association with CD31 throughout the tumor, irrespective of trastuzumab saturation (Fig. 3C). Vascular maturity is also thought to have a significant impact on the stability of tumor vasculature, where pericytes, among other things, regulate vascular diameter and permeability (35, 36). A trend of fewer microvessels associated with pericytes is found in sections located toward the center of tumors relative to proximal sections (Fig. 3D), which corresponds to higher trastuzumab saturation in the same sections. No exploration into this association was done in this study, and these data are not considered evidence of a causal relationship. It is plausible, however, that more mature vessels, as indicated by presence of pericytes, could have improved efficiency in delivery of macromolecules to tumor tissue, and further investigations based on this preliminary data may be warranted.

There are multiple reports supporting the binding site barrier hypothesis first proposed by Weinstein et al., which suggests that high antibody affinity and high expression levels of antigen will hinder the penetration of an antibody through tumor tissue via its own successful binding to antigen (37–39). In the present study, examination of trastuzumab at progressive time points in this highly overexpressing HER2 model showed that, with time, trastuzumab is able to reach some cells located far from vasculature. Those vessels associated with poor extravascular distribution of trastuzumab did not exhibit noticeably more or less HER2 expression in perivascular cells, suggesting that the degree of associated trastuzumab is not the result of variable HER2 expression.

Elevated interstitial fluid pressure in tumors has also been suggested as partially responsible for poor monoclonal antibody penetration (3, 40, 41), particularly in the tumor core, where high interstitial fluid pressure principally prevents macromolecular extravasation and also influences interstitial fluid convection. Tumor vessels are otherwise thought to be sufficiently permeable and leaky that the limiting factor for extravasation will be blood flow (42, 43). As also indicated above, Fig. 4 illustrates that at both early and late time points, trastuzumab was found extravasating from blood vessels in the central regions of tumors, as well as at the periphery in a heterogeneous pattern not isolated to large geographic regions, such as the rim or core.

Factors not considered in this study include rate of blood flow, vascular permeability, and tumor tissue interstitial components that would affect convection and the interstitial diffusion coefficient of trastuzumab. Notwithstanding considerable heterogeneity in trastuzumab distribution in the doses and time points examined, the ability of trastuzumab to penetrate through tissue with time seems relatively efficient in consideration of its high molecular weight and high binding affinity. In most studies evaluating the efficacy of trastuzumab, the therapeutic regimen would involve multiple doses and in combination with its long plasma half life, based on these results, it is plausible that trastuzumab would eventually have the opportunity to access most target cells within a solid tumor. Importantly, however, complete saturation of HER2 binding sites throughout the tumor was not seen in our study, and it is not clear what inhibited its complete distribution. This could have a significant effect on the success of cancer therapy wherein survival of individual cells can lead to tumor repopulation. Further studies examining distribution of trastuzumab after prolonged therapy and investigation of relative changes in pharmacodynamic markers between regions with and without bound trastuzumab could provide clarity regarding whether poor tumor tissue penetration is a mechanism for resistance to trastuzumab.

Acknowledgments

The authors wish to gratefully acknowledge Drs. Corinna Warburton and Wieslawa Dragowska for providing us with the LCC6 tumor models.

References

1. Minchinton AI, Tannock IF. Drug penetration in solid tumours. Nat Rev Cancer 2006;6:583–92.

2. Carmeliet P, Jain RK. Angiogenesis in cancer and other diseases. Nature 2000;407:249–57.

3. Jain RK. Physiological barriers to delivery of monoclonal antibodies and other macromolecules in tumors. Cancer Res 1990;50:814s–9.

4. Baluk P, Morikawa S, Haskell A, Mancuso M, McDonald DM. Abnormalities of basement membrane on blood vessels and endothelial sprouts in tumors. Am J Pathol 2003;163:1801–15.

5. Netti PA, Berk DA, Swartz MA, Grodzinsky AJ, Jain RK. Role of extracellular matrix assembly in interstitial transport in solid tumors. Cancer Res 2000;60:2497–503.

6. Wiig H, Gyenge CC, Tenstad O. The interstitial distribution of macromolecules in rat tumours is influenced by the negatively charged matrix components. J Physiol 2005;567:557–67.

7. Coussens LM, Werb Z. Inflammation and cancer. Nature 2002;420:860–7.

8. Menard S, Casalini P, Campiglio M, Pupa S, Agresti R, Tagliabue E. HER2 overexpression in various tumor types, focussing on its relationship to the development of invasive breast cancer. Ann Oncol 2001;12 Suppl 1:S15–9.

9. Borst P, Evers R, Kool M, Wijnholds J. A family of drug transporters: the multidrug resistance-associated proteins. J Natl Cancer Inst 2000;92:1295–302.

10. Primeau AJ, Rendon A, Hedley D, Lilge L, Tannock IF. The distribution of the anticancer drug Doxorubicin in relation to blood vessels in solid tumors. Clin Cancer Res 2005;11:8782–8.

11. Huxham LA, Kyle AH, Baker JH, Nykilchuk LK, Minchinton AI. Microregional effects of gemcitabine in HCT-116 xenografts. Cancer Res 2004;64:6537–41.

12. Kyle AH, Huxham LA, Yeoman DM, Minchinton AI. Limited tissue penetration of taxanes: a mechanism for resistance in solid tumors. Clin Cancer Res 2007;13:2804–10.

13. Holliger P, Hudson PJ. Engineered antibody fragments and the rise of single domains. Nat Biotechnol 2005;23:1126–36.

14. Reichert JM, Valge-Archer VE. Development trends for monoclonal antibody cancer therapeutics. Nat Rev Drug Discov 2007;6:349–56.

15. Hudis CA. Trastuzumab-mechanism of action and use in clinical practice. N Engl J Med 2007;357:39–51.

16. Baselga J, Perez EA, Pienkowski T, Bell R. Adjuvant trastuzumab: a milestone in the treatment of HER-2-positive early breast cancer. Oncologist 2006;11:4–12.

17. Mass RD, Press MF, Anderson S, et al. Evaluation of clinical outcomes according to HER2 detection by fluorescence *in situ* hybridization in women with metastatic breast cancer treated with trastuzumab. Clin Breast Cancer 2005;6:240–6.

18. Piccart-Gebhart MJ, Procter M, Leyland-Jones B, et al. Trastuzumab after adjuvant chemotherapy in HER2-positive breast cancer. N Engl J Med 2005;353:1659–72.

19. Glazyrin A, Shen X, Blanc V, Eliason JF. Direct detection of herceptin/trastuzumab binding on breast tissue sections. J Histochem Cytochem 2007;55:25–33.

20. Adams GP, Schier R, McCall AM, et al. High affinity restricts the localization and tumor penetration of single-chain Fv antibody molecules. Cancer Res 2001;61:4750–5.

21. Grossi PM, Ochiai H, Archer GE, et al. Efficacy of intracerebral microinfusion of trastuzumab in an athymic rat model of intracerebral metastatic breast cancer. Clin Cancer Res 2003;9:5514–20.

22. Dennis MS, Fau-Jin H, Jin H, et al. Imaging tumors with an albumin-binding Fab, a novel tumor-targeting agent. Cancer Res 2007;67:254–61.

23. Palm S, Enmon RM, Jr., Matei C, et al. Pharmacokinetics and biodistribution of 86Y-trastuzumab for 90Y dosimetry in an ovarian carcinoma model: correlative MicroPET and MRI. J Nucl Med 2003;44:1148–55.

24. Kobayashi H, Shirakawa K, Kawamoto S, et al. Rapid accumulation and internalization of radiolabeled herceptin in an inflammatory breast cancer xenograft with vasculogenic mimicry predicted by the contrast-enhanced dynamic MRI with the macromolecular contrast agent G6-(1B4M-Gd)256. Cancer Res 2002;62:860–6.

25. Tada H, Higuchi H, Wanatabe TM, Ohuchi N. *In vivo* real-time tracking of single quantum dots conjugated with monoclonal anti-HER2 antibody in tumors of mice. Cancer Res 2007;67:1138–44.

26. Trotter MJ, Chaplin DJ, Olive PL. Use of a carbocyanine dye as a marker of functional vasculature in murine tumours. Br J Cancer 1989;59:706–9.

27. Warburton C, Dragowska WH, Gelmon K, et al. Treatment of HER-2/neu overexpressing breast cancer xenograft models with trastuzumab (Herceptin) and gefitinib (ZD1839): drug combination effects on tumor growth, HER-2/neu and epidermal growth factor receptor expression, and viable hypoxic cell fraction. Clin Cancer Res 2004;10:2512–24.

28. Rae J, Creighton C, Meck J, Haddad B, Johnson M. MDA-MB-435 cells are derived from M14 Melanoma cells-a loss for breast cancer, but a boon for melanoma research. Breast Cancer Res Treat 2007;104:13–9.

29. Lub-de Hooge MN, Kosterink JG, Perik PJ, et al. Preclinical characterisation of 111In-DTPA-trastuzumab. Br J Pharmacol 2004;143:99–106.

30. Tang Y, Scollard D, Chen P, et al. Imaging of HER2/neu expression in BT-474 human breast cancer xenografts in athymic mice using [99mTc]-HYNIC-trastuzumab (Herceptin) Fab fragments. Nucl Med Commun 2005;26:427–32.

31. Baselga J, Norton L, Albanell J, Kim YM, Mendelsohn J. Recombinant humanized anti-HER2 antibody (Herceptin) enhances the antitumor activity of paclitaxel and doxorubicin against HER2/neu overexpressing human breast cancer xenografts. Cancer Res 1998;58:2825–31.

32. Mandler R, Kobayashi H, Hinson ER, Brechbiel MW, Waldmann TA. Herceptin-geldanamycin immunoconjugates: pharmacokinetics, biodistribution, and enhanced antitumor activity. Cancer Res 2004;64:1460–7.

33. Durand RE. Intermittent blood flow in solid tumours-an under-appreciated source of 'drug resistance.' Cancer Metastasis Rev 2001;20:57–61.

34. Choi J, Credit K, Henderson K, et al. Intraperitoneal immunotherapy for metastatic ovarian carcinoma: resistance of intratumoral collagen to antibody penetration. Clin Cancer Res 2006;12:1906–12.

35. Jain RK. Molecular regulation of vessel maturation. Nat Med 2003;9:685–93.

36. Morikawa S, Baluk P, Kaidoh T, Haskell A, Jain RK, McDonald DM. Abnormalities in pericytes on blood vessels and endothelial sprouts in tumors. Am J Pathol 2002;160:985–1000.

37. Weinstein JN, van Osdol W. Early Intervention in Cancer Using Monoclonal antibodies and other biological ligands: micropharmacology and the ''binding site barrier.'' Cancer Res 1992;52:2747s–51.

38. Saga T, Neumann RD, Heya T, et al. Targeting cancer micrometastases with monoclonal antibodies: a binding-site barrier. Proc Natl Acad Sci U S A 1995;92:8999–9003.

39. Juweid M, Neumann R, Paik C, et al. Micropharmacology of monoclonal antibodies in solid tumors: direct experimental evidence for a binding site barrier. Cancer Res 1992;52:5144–53.

40. Flessner MF, Choi J, Credit K, Deverkadra R, Henderson K. Resistance of tumor interstitial pressure to the penetration of intraperitoneally delivered antibodies into metastatic ovarian tumors. Clin Cancer Res 2005;11:3117–25.

41. Jain RK, Baxter LT. Mechanisms of heterogeneous distribution of monoclonal antibodies and other macromolecules in tumors: significance of elevated interstitial pressure. Cancer Res 1988;48:7022–32.

42. McDonald DM, Baluk P. Significance of blood vessel leakiness in cancer. Cancer Res 2002;62:5381–5.

43. Yuan F, Dellian M, Fukumura D, et al. Vascular permeability in a human tumor xenograft: molecular size dependence and cutoff size. Cancer Res 1995;55:3752–6.